

Supporting Information

Template-free scalable growth of vertically aligned MoS₂ nanowire arrays meta-structural films towards robust superlubricity

Jing Shi,^{a,b} Runqiang Zhao,^a Zaixiu Yang,^c Jinzhu Yang,^d Wenhe Zhang,^d Chengbing Wang,^{*d}
Junyan Zhang,^{*c}

^a College of Mechanical & Electrical Engineering, Shaanxi University of Science & Technology, Xi'an, Shaanxi 710021, China

^b State Key Laboratory of Tribology, Tsinghua University, Beijing 100084, China

^c Key Laboratory of Science and Technology on Wear and Protection of Materials, Lanzhou Institute of Chemical Physics, Chinese Academy of Sciences, Lanzhou 730000, China

^d School of Materials Science and Engineering, Shaanxi Key Laboratory of Green Preparation and Functionalization for Inorganic Materials, Shaanxi University of Science and Technology, Xi'an, Shaanxi 710021, China

This PDF file includes:

Section 1 and 2

Figs. S1 to S11

Tables S1 to S4

References (1 to 4)

Section 1. Density functional theory simulations.

Since the (111) plane of Ag with low surface energy is a widely observed experimental stable surface,¹ the interfacial properties against MoS₂ were also investigated in this paper based on the bulk Ag. Since lattice mismatch between the lattice of 3.050 Å for Ag (111) and 3.281 Å for MoS₂ was 7%, and dislocation may occur at the interface, the Ag/MoS₂ interface was constructed by considering the lattice of MoS₂ rotated by 30° in (002) plane (MoS₂R30 lattice: 5.683 Å) and lattice of Ag (111) rotated by 13.9° (AgR13.9 lattice: 10.996 Å). Thus, the interface was constructed by matching the (1 × 1) cell of AgR13.9 with eight layers of Ag to a (2 × 2) cell of monolayer MoS₂R30 with the lattice of 11.366 Å, where the lattice mismatch between MoS₂ and Ag of 3% inhibits dislocations at the interface. The interface was added with a 15 Å vacuum layer in the direction normal to the interface to calculate the interlayer binding energy (E_B) and exclude interaction from adjacent images. Moreover, the bottom Ag layer was fixed to represent the bulk properties of Ag. The E_B was calculated from $E_B = (E_{\text{Interface}} - E_{\text{Layer1}} - E_{\text{Layer2}})/A$, where the $E_{\text{Interface}}$, E_{Layer1} , and E_{Layer2} are total energies for the interface and isolated layers. For comparison, the adsorption behavior of an Ag atom on the (002) basal plane of monolayer MoS₂ was also investigated in the same cell by using a k-point grid of 4 × 4 × 1. The interfacial sliding behavior of the Ag/MoS₂ interface in the same cell was also studied to rational low friction behavior of the VO-Ag/MoS₂ film. The top MoS₂ layer in the interface with its top S layer fixed in x and y directions is gradually shifted in the x direction by 5.683 Å with an interval of 0.3 Å. The interfacial sliding of bilayer MoS₂ in the same cell was also investigated by fixing the lowest layer of S from the bottom MoS₂ layer in all directions, and the highest layer of S from the top MoS₂ layer fixed in x and y directions and shifted in the x direction using the same methodology.

Section 2. Deposition of VO–A and P–MoS₂ films.

In this paper, a focus is placed on the crystal quality affected by the substrate temperature T_{sub} . Films grown without external heating have nanoparticles with irregular sphericities distributed on the surface, and the particle diameter covers the range from ~150 nm to ~500 nm. Moreover, the EDS point-scanning on nanoparticle and non-particle region reveals that the particle has a higher Ag concentration (34.64%) than the non-particle region (20.26%). With an increase in T_{sub} , the film surface becomes densely packed without nanoparticles, composed of Ag, Mo, and S. Consequently, surface roughness is reduced from 5.394 nm to 3.236 nm.

According to classic Thornton's model, sputtered bulk film usually has two typical crystallographic orientations: *Type-I* (basal plane vertical to the substrate) and *Type-II* (basal plane parallel to the substrate). *Type-I* has porous or columnar structure characteristics and exposes large amounts of reactive edge sites, consequently having high friction. *Type-II* has densely packed fibrous grain characteristics and exhibits low friction but weak adhesion to the substrate. This is synergistically dependent on the applied direct current bias, Joule heating on the substrate, and the pre-deposited transition layer. The parameters were optimized with a rational P/T (working pressure/substrate Joule heating temperature) ratio and negative bias on substrates. Moreover, the nc–Ag pinning role is indispensable. As a comparison, pure MoS₂ films (P–MoS₂) were deposited with comparable parameters of VO–A films on silicon substrates. The samples are marked with P–MoS₂–0, P–MoS₂–100, P–MoS₂–150, P–MoS₂–200, P–MoS₂–250, and P–MoS₂–300. Without the pinning effect of nc–Ag, the films are porous and worm-like (Figure S8, Figure S9). This indicates that the nc–Ag NPs have vital roles in forming the metastructure of the VO NWAs.

Typically, MoS₂ films deposited via chemical vapor deposition usually have substrate-parallel orientation, which requires the support of graphene sheets. Furthermore, the thick film is initially grown from isolated triangular grains.² Moreover, PVD can be employed to prepare

pure MoS₂ film or MoS₂/C composite film. However, the MoS₂ orientation is still parallel or desultory.^{3,4} In this work, the as-grown VO-A metamaterial film exhibits a new *T*-type morphology with vertical orientation inside but parallel orientation near the surface region. In addition to nc-MoS₂, both nc-Ag and a-MoS_{2-x}O_x matrices exist near the film surface.

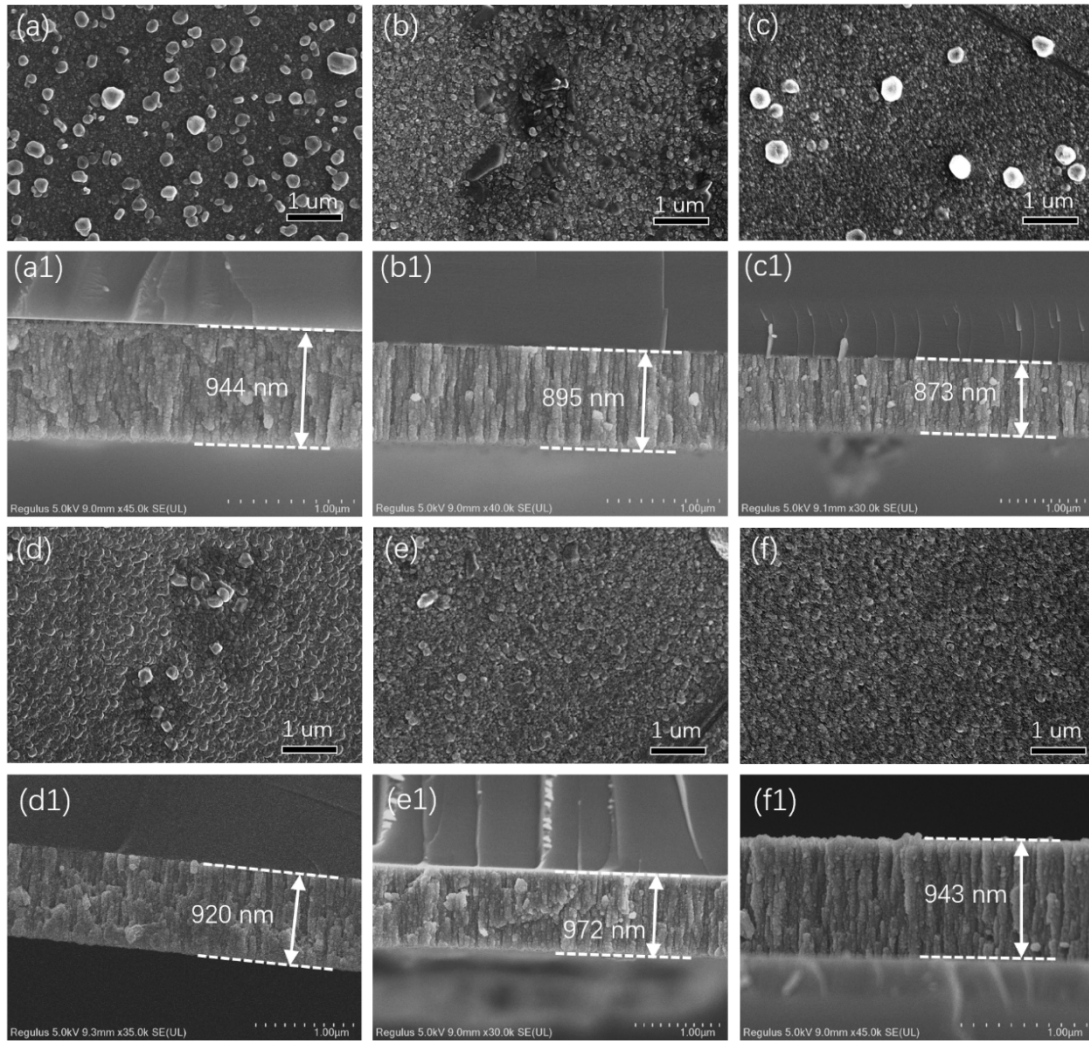


Fig. S1 Surface and cross-sectional topography SEM images of VO–MoS₂ MWAs meta-structural films deposited at different substrate temperature of (a, a1) unheated, (b, b1) 100 °C, (c, c1) 150 °C, (d, d1) 200 °C, (e, e1) 250 °C, and (f, f1) 300 °C, respectively.

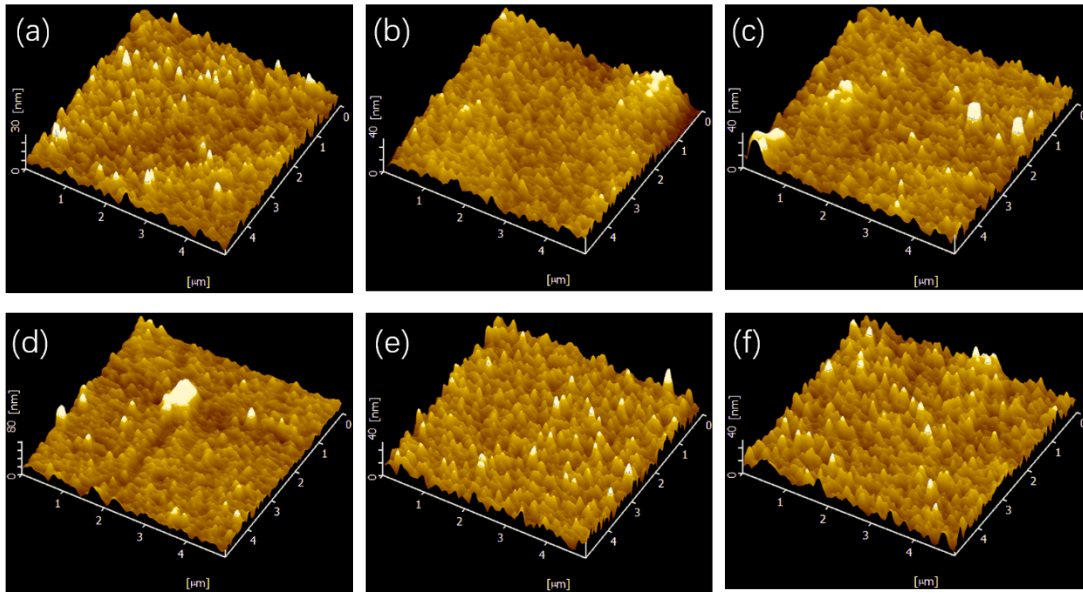


Fig. S2 AFM 3D $5 \times 5 \mu\text{m}^2$ profile images for VO-MoS₂ MWAs meta-structural films deposited at different substrate temperature of: (a) unheated, (b) 100 °C, (c) 150 °C, (d) 200 °C, (e) 250 °C, and (f) 300 °C, respectively.

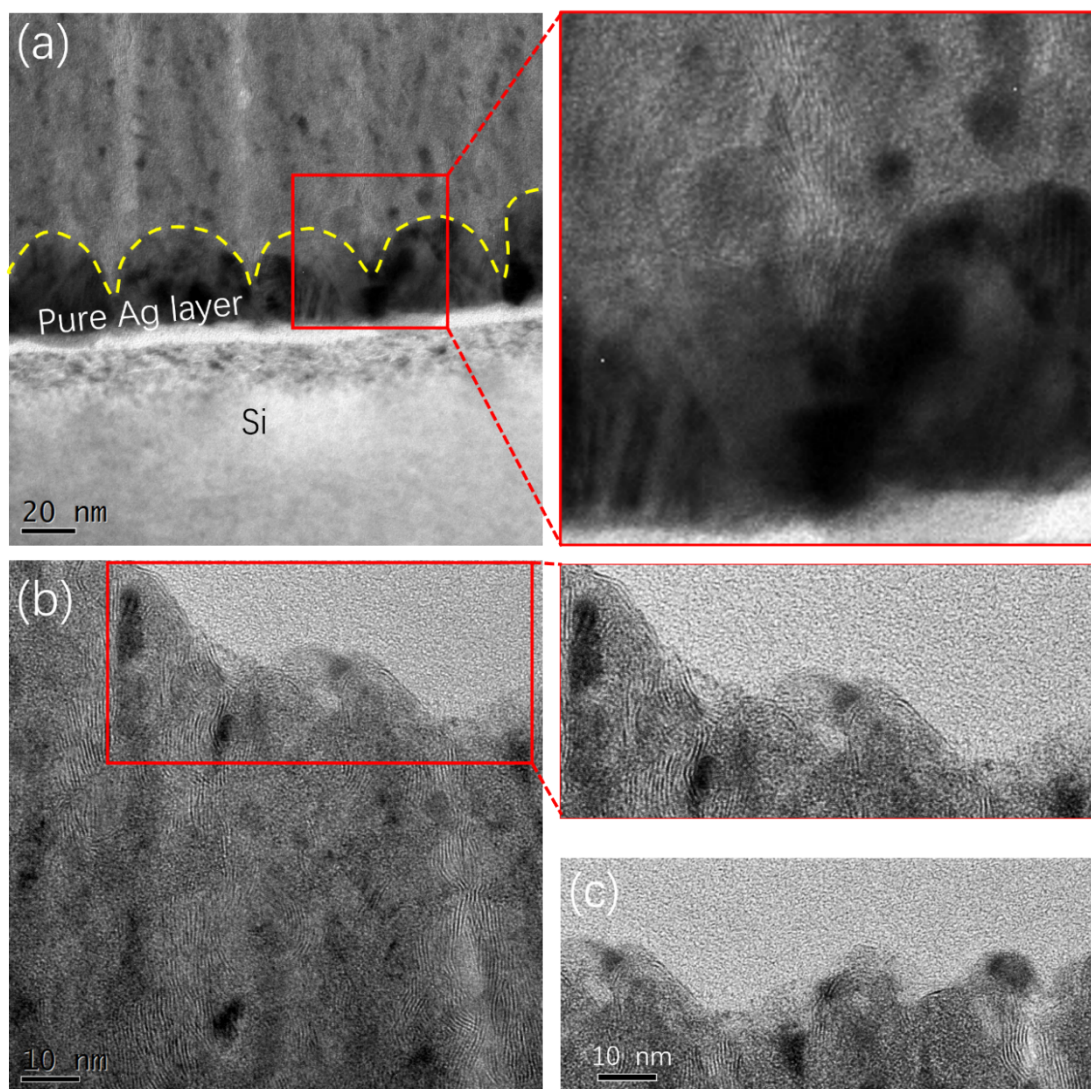


Fig. S3 (a) Enlarged HRTEM image of the connecting region between nc-Ag layer and VO-MoS₂ NWAs in Figure 1g. (b, c) Enlarged HRTEM images of parallel-oriented MoS₂ basal planes at the near surface regions in Figure 1i.



Fig. S4 High resolution TEM image of pure MoS₂ film with amorphous nano-structure.

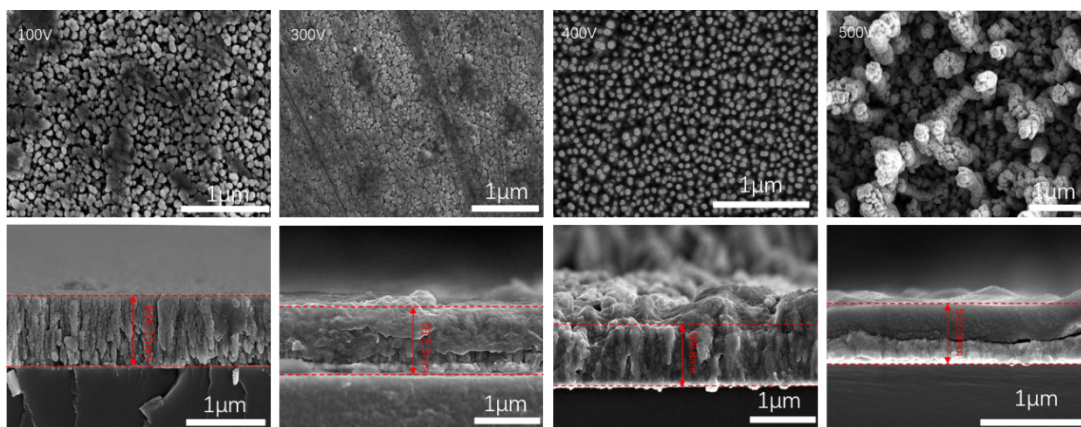


Fig. S5 Surface and cross-sectional topography SEM images of VO-As films deposited at comparable parameters with VO-A250 and negative bias changed from -100 V to -500 V.

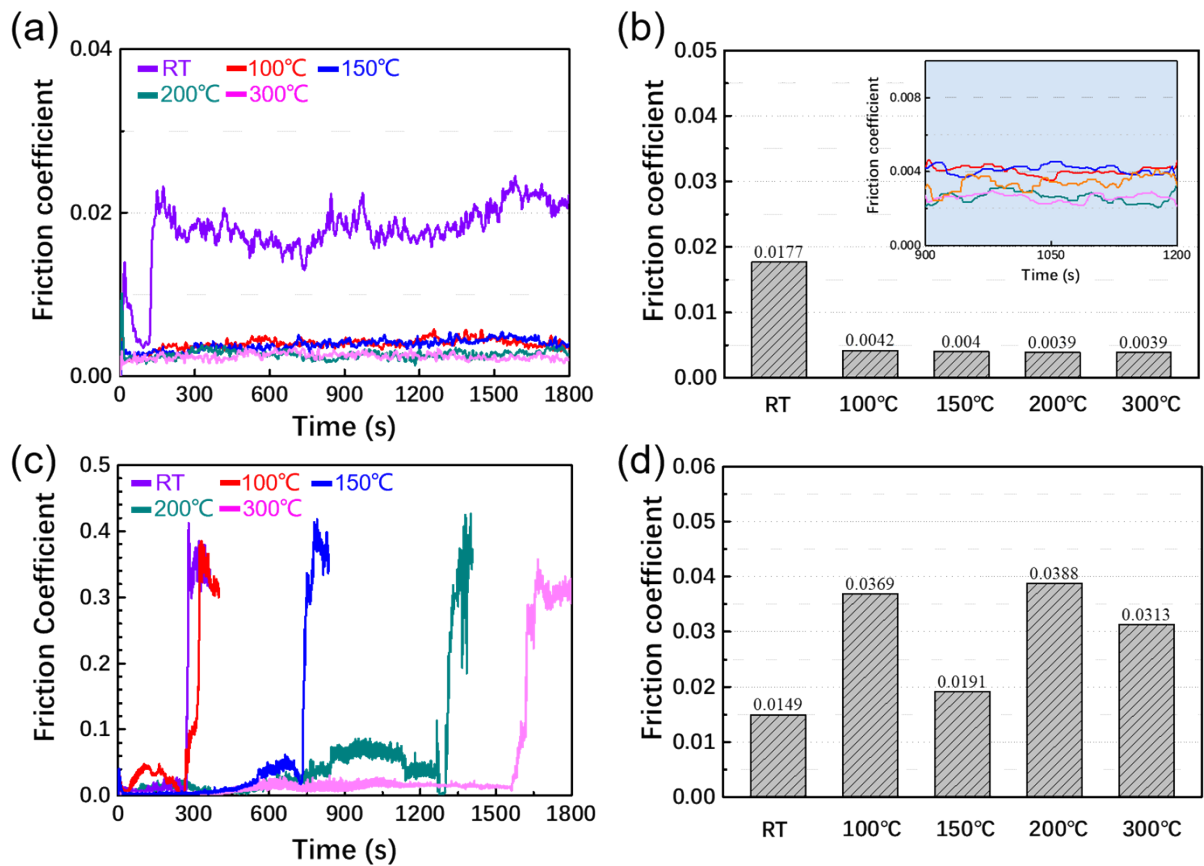


Fig. S6 (a) Friction curves and (b) calculated stable friction coefficient μ of VO-MoS₂ MWAs meta-structural films correspond to extra substrate temperature of unheated, 100 °C, 150 °C, 200 °C, and 300 °C, respectively. The inset shows enlarged steady state friction curves from Figure S4a. (c) Friction curves and (d) calculated stable friction coefficient μ of P-MoS₂-0, P-MoS₂-100, P-MoS₂-150, P-MoS₂-200, and P-MoS₂-300 films fabricated with an extra substrate temperature of unheated, 100 °C, 150 °C, 200 °C, and 300 °C, respectively.

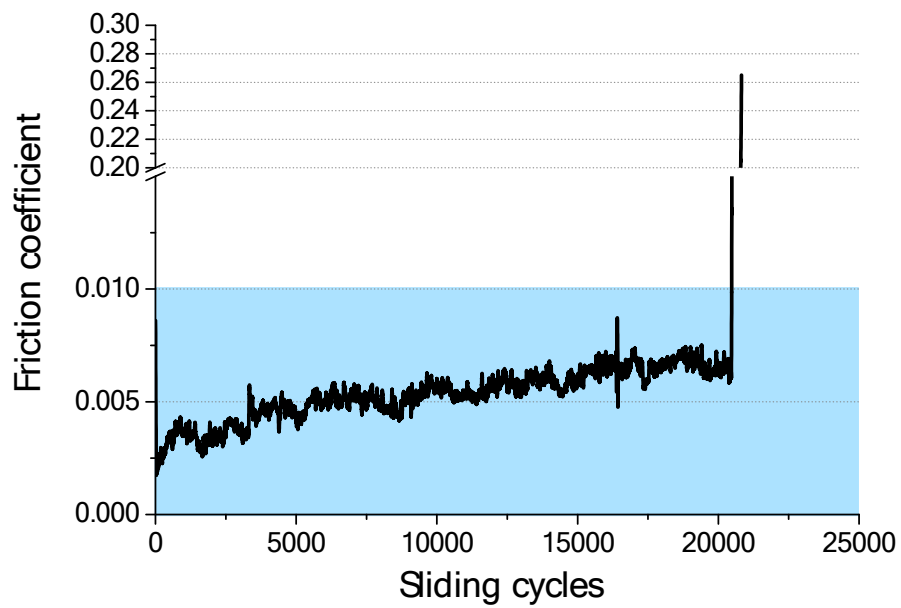


Fig. S7 Superlubricity life testing of VO-A250 in ambient atmosphere. The superlubricity (friction coefficient lower than 0.0053) shows robustness within 20400 cycles.

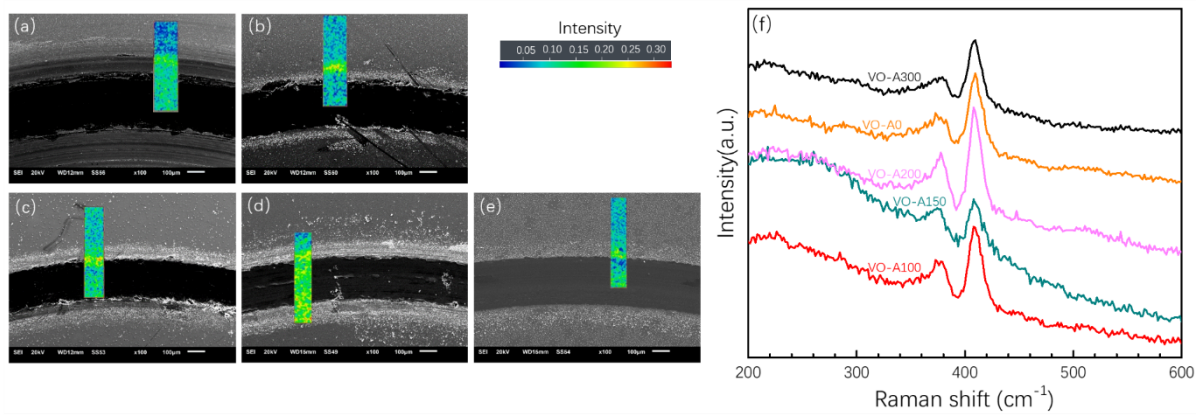


Fig. S8 Raman spectra 2D mapping of wear tracks on VO–MoS₂ MWAs meta-structural films deposited at different substrate temperature of: (a) unheated, (b) 100 °C, (c) 150 °C, (d) 200 °C, and (e) 300 °C, respectively.

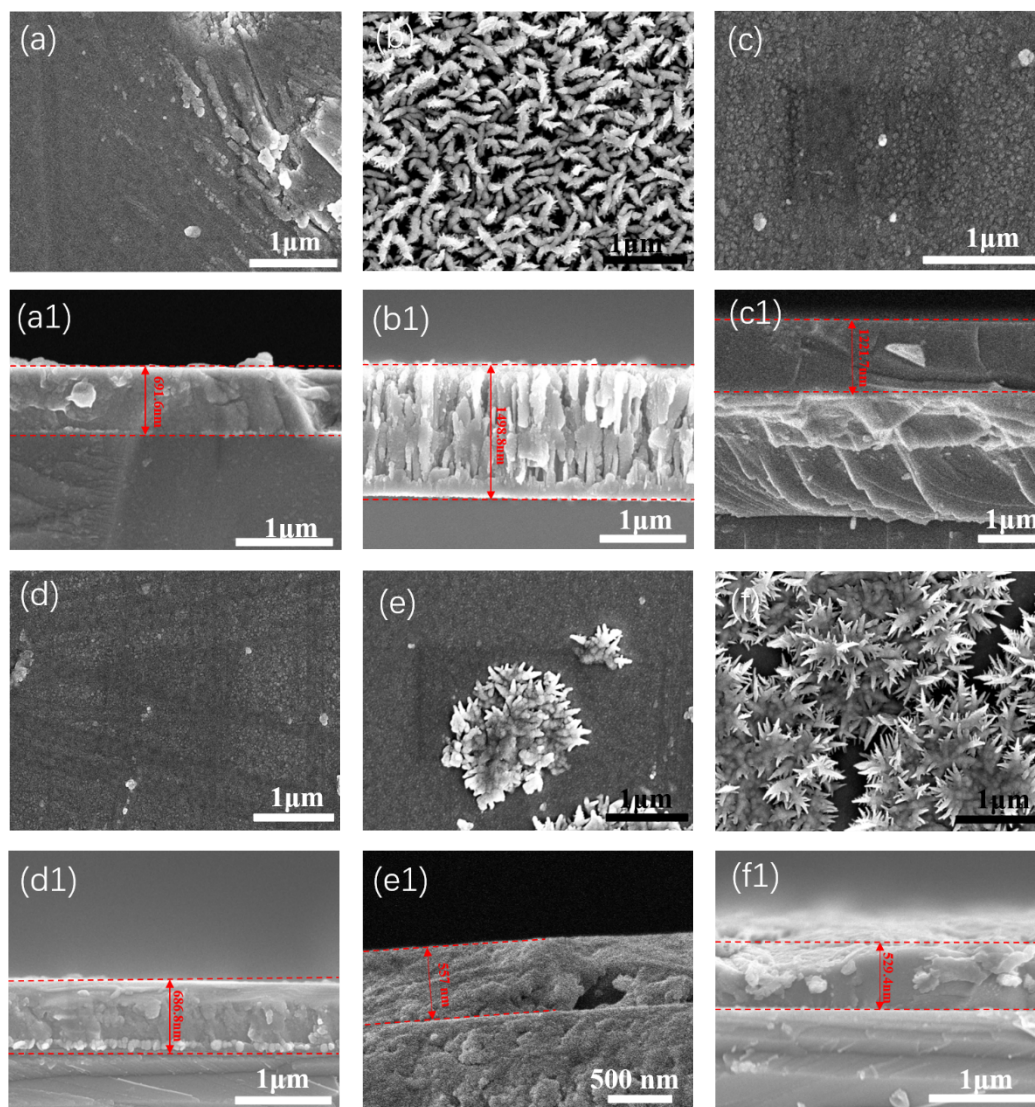


Fig. S9 Surface and cross-sectional topography SEM images of pure MoS₂ films (P-MoS₂) deposited at comparable parameters: (a, a1) P-MoS₂-0, (b, b1) P-MoS₂-100, (c, c1) P-MoS₂-150, (d, d1) P-MoS₂-200, (e, e1) P-MoS₂-250, and (f, f1) P-MoS₂-300.

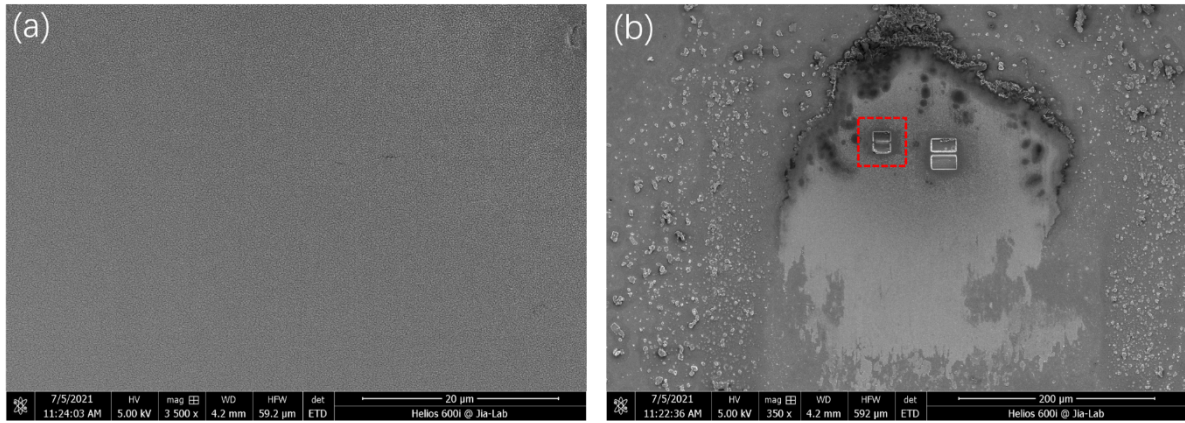


Fig. S10 FIB-SEM image of tribofilm from VO-A250 (VO-MoS₂ MWAs meta-structural films deposited at 250 °C): (a) before, and (b) after FIB milling.

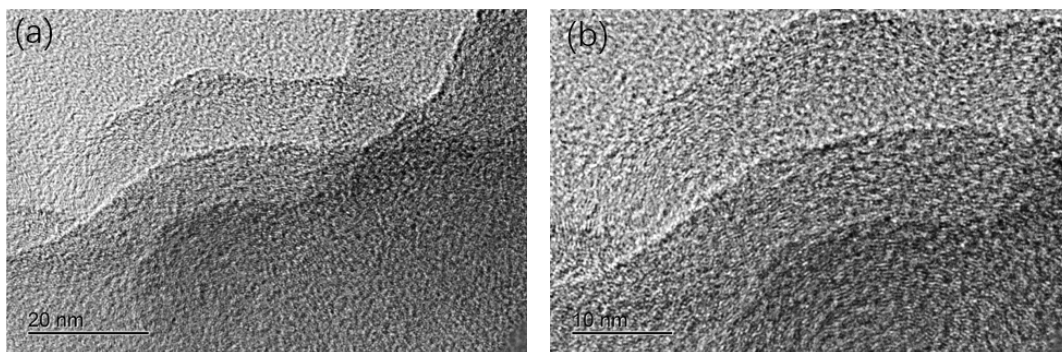


Fig. S11 TEM images of wear debris collected from the counterpart wear scar of P-MoS₂-250.

Table S1. The Raman peak parameters for wear tracks on film in VO-A0, VO-A100, VO-A150, VO-A200, VO-A250, and VO-A300 films.

	E_{2g}^1 peak center position (cm^{-1})	E_{2g}^1 peak FWHM (cm^{-1})	A_{1g} peak center position (cm^{-1})	A_{1g} peak FWHM (cm^{-1})	$I(E_{2g}^1)/I(A_{1g})$	Frequency difference (cm^{-1})
VO-A0	373.48	21.75	408.93	15.30	0.61/0.433	35.45
VO-A100	374.38	22.58	409.93	14.60	0.64/0.411	35.55
VO-A150	373.46	18.28	410.86	18.44	0.51/0.52	37.40
VO-A200	374.72	20.98	409.74	13.79	0.62/0.41	35.02
VO-A250	371.96	32.09	410.03	15.69	0.73/0.36	38.04
VO-A300	372.64	35.41	409.38	15.42	0.76/0.33	36.74

Table S2. Interlayer binding energies (E_b) and the interlayer spacing (d) values of MoS₂ bilayers, with different layer stacking configurations. The effects of dissociation of H₂O and adsorption of undissociated H₂O are shown.

MoS ₂ bilayer structures	Surface and interface with or without dissociated H ₂ O		Interface with adsorbed undissociated H ₂ O		
	d (Å)	E_b (J/m ²)	d (Å)	E_b (J/m ²)	E_a (eV)
Pristine AA	6.89	0.23			
Pristine A'B	6.88	0.23			
Pristine AA'	6.44	0.31	7.03	0.16	1.32
Pristine AB	6.40	0.31	7.33	0.16	1.33
Pristine AB'	6.46	0.30	6.38	0.37	-0.75
AA': H-D-MoS ₂ / D-MoS ₂ -H	6.38	0.29	6.38	0.37	-0.75

Table S3. Energy barrier for the sliding of the Ag/MoS₂ at different sliding distances compared with that for MoS₂/MoS₂ initiated from AA' stack (distance A = 0 Å, distance A' = 5.683 Å).

Distance (Å)	Energy barrier (eV)	
	Ag/MoS ₂	MoS ₂ /MoS ₂
0	-4.10×10 ⁻⁵	0
0.28415	-0.00147	0.02708
0.5683	-0.00113	0.08093
0.85245	-0.00178	0.11865
1.1366	-0.00213	0.12981
1.42075	-0.0018	0.11402
1.7049	-0.00194	0.08039
1.98905	-0.00142	0.07363
2.2732	-9.42×10 ⁻⁴	0.12752
2.55735	-0.00213	0.22614
2.8415	-0.00207	0.34216
3.12565	-0.0017	0.43724
3.4098	-0.00179	0.50258
3.69395	-0.00163	0.53175
3.9781	-0.00164	0.52665
4.26225	-0.00153	0.48015
4.5464	-0.00137	0.39795
4.83055	-7.00×10 ⁻⁶	0.279
5.1147	-6.50×10 ⁻⁴	0.14269
5.39885	-8.37×10 ⁻⁴	0.03672
5.683	-4.10×10 ⁻⁵	1.00×10 ⁻⁵

Table S4. Deposition parameter details, thickness, and surface roughness of as-grown films. Vertically oriented Ag–MoS₂ films are denoted as “VO–A.” The total thickness of the film is observed via cross-sectional SEM images, and the surface roughness is determined by AFM.

No.	VO-A0	VO-A100	VO-A150	VO-A200	VO-A250	VO-A300
Temperature (°C)	Non-heated	100	150	200	250	300
Ag nano-islands layer	Working pressure (Pa)	0.6	0.6	0.6	0.6	0.6
	Power (W)	60	60	60	60	60
	Ar (sccm)	100	100	100	100	100
	Time (min)	15	15	15	15	15
	Ag target voltage (V)	229	227	229	228	233
VO-Ag/MoS ₂ layer	Ag target current (A)	0.018	0.018	0.018	0.018	0.018
	MoS ₂ target power (W)	200	200	200	200	200
	Ar (sccm)	108	108	108	108	108
	Time (min)	90	90	90	90	90
Negative bias (V)	200 V	200 V	200 V	200 V	200 V	200 V
Film total thickness (nm)	944	895	873	920	972	943
Film surface roughness (nm)	3.236	5.208	4.558	5.532	4.983	5.394

References

- (1) Yamamoto, S.; Yoshida, Y.; Imada, H.; Kim, Y.; Hasegawa, Y. Direct Visualization of Surface Phase of Oxygen Molecules Physisorbed on Ag (111) Surface: A Two-Dimensional Quantum Spin System. *Physical Review B*, **2016**, *93*, 081408.
- (2) Cheng, J.; Shen, C.; He, Y.; Wei, H.; Liu, S.; Qiu, P.; Song, Y.; Wei S.; Wang, Z.; Zheng, X.; Peng, M. Reaction Mechanism Transformation of LPCVD-Grown MoS₂ from Isolated Triangular Grains to Continuous Films. *Journal of Alloys and Compounds*, **2021**, *853*, 157374.
- (3) Duan, Z.; Zhao, X.; Xu, J.; Wang, P.; Liu, W. Influence of Ni¹³⁺ Ions Irradiation on the Microstructure, Mechanical and Tribological Properties of Mo-S-Ti Composite Films. *Applied Surface Science*, **2019**, *480*, 438-447.
- (4) Gong, Z.; Jia, X.; Ma, W.; Zhang, B.; Zhang, J. Hierarchical Structure Graphitic-Like/MoS₂ Film as Superlubricity Material. *Applied Surface Science*, **2017**, *413*, 381-386.